Article

Discovery Medicine 2025; 37(194): 535–541
https://doi.org/10.24976/Discov.Med.202537194.45

Structural Changes in Membrane Dynamics under the Action of Miltefosine

Irina Georgieva[1], Sonia Apostolova[1], Teodora Vukova[1], Kostadin Kostadinov[2], Rumiana Tzoneva[1,*]

[1]Transmembrane Signaling Laboratory, Institute of Biophysics and Biomedical Engineering, Bulgarian Academy of Sciences, 1113 Sofia, Bulgaria
[2]Institute of Mechanics, Bulgarian Academy of Sciences, 1113 Sofia, Bulgaria
*Correspondence: tzoneva@bio21.bas.bg (Rumiana Tzoneva)
Published: 20 March 2025

Background: Miltefosine, an alkylphosphocholine, affects lipid metabolism and cell signaling by interacting with cell membranes. In this study, we aim to demonstrate the effect of miltefosine (hexadecylphosphocholine (HePC)) on the alterations of the membrane lipid content of human lung adenocarcinoma (A549) cells and normal human umbilical vein endothelial cells (HUVECs) in respect to the reduction of their membrane fluidity and metastatic potential of the cancer cells.

Methods: To study lateral diffusion in cell membranes, we employed membrane labeling with fusogenic liposomes followed by fluorescence recovery after photobleaching (FRAP) analysis. Cell viability was examined by 3-(4,5-dimethylthiazol-2-yl)-2,5-diphenyl-2H-tetrazolium bromide (MTT) assay; total cholesterol and sphingomyelin were measured using commercially available kits.

Results: Miltefosine inhibited cell growth and increased the total cholesterol in both cell lines ($p < 0.05$ for HUVEC and $p < 0.01$ for A549). Sphingomyelin levels were not significantly altered in A549 cells, but in HUVECs HePC caused a decrease in sphingomyelin ($p < 0.05$). Miltefosine treatment of A549 cells reduced the membrane diffusion coefficient ($p < 0.001$), which was associated with an increased half-time of fluorescent recovery ($p < 0.05$) measured by FRAP. These changes reflect a significant reduction in membrane fluidity in the cancer cells. In contrast, miltefosine induced a milder response in HUVECs, attenuating the diffusion coefficient ($p < 0.05$) but not affecting the half-time of fluorescent recovery. As a result, the reduction in membrane fluidity in HUVECs was less pronounced.

Conclusion: Miltefosine induces a decrease in membrane fluidity of cancer cells, and this effect was related to decreased cell viability and total cholesterol levels. Miltefosine may be an effective antitumor agent and has great potential as an adjuvant therapy in the future.

Keywords: miltefosine; membrane fluidity; FRAP; cancer cells; non-cancer cells

Introduction

Compartmentalization of cellular structures is achieved by a phospholipid bilayer, which forms the cellular membrane and maintains the integrity of each cell and its organelles. The membrane is highly dynamic due to the constant motion of proteins and lipids, a phenomenon known as membrane fluidity, which describes the lateral diffusion of membrane lipids [1]. Cells adjust to their environment by altering their chemical composition and physical properties; thus, membrane fluidity can indicate proper membrane function and cell viability. Cancer cells often exhibit higher membrane fluidity compared to normal cells [2]. Consequently, drugs targeting the cell membrane are considered as promising cancer therapeutics. Alkylphosphocholines (APCs) are a unique class of selective antitumor lipids that target cell membranes rather than the nucleus, unlike conventional cytostatics [3,4]. Miltefosine (hexadecylphosphocholine (HePC)), the only APC currently used in clinical practice, is primarily employed to treat leishmaniasis [5]. Research into the interaction of miltefosine has highlighted its selective effects on lipid membranes mimicking cancer and healthy cells. Model membrane systems, including Dipalmitoylphosphatidylcholine (DPPC) and 1,2-Dipalmitoyl-sn-glycero-3-phosphoserine, sodium salt (DPPS) multilamellar and large unilamellar vesicles, have been employed to study these interactions [6,7]. HePC demonstrates a pronounced affinity for DPPS-rich membranes, which mimic cancer cells, compared to DPPC-based systems, which are representative of healthy cell membranes. In DPPS/HePC systems, HePC facilitates deeper penetration into the lipid tails and increases lipid-drug interactions while in DPPC/HePC systems HePC promotes lipid order without significant disruption [6]. Additionally, HePC expands the phase

transition range of DPPS membranes significantly more than DPPC membranes, indicating stronger interaction with cancer-like lipid compositions [6]. These findings correlate with studies showing that HePC increases membrane fluidity in certain model systems and selectively targets cancer cells over healthy cells [6,8]. Together, this molecular-level evidence underscores HePC's potential as a selective antitumor agent by modulating membrane dynamics [6–8]. However, an understanding of the direct effect of HePC on membrane fluidity in living cells is currently lacking. Our lab previously demonstrated its potent anticancer effects; HePC induces apoptosis in the human lung adenocarcinoma (A549) cell line and leads to a decrease in the amount of sphingosine-1-phosphate, a lipid that supports cell survival [9]. Additionally, we found that erufosine, another APC, increased membrane disorder in breast cancer cell lines [10], further highlighting the therapeutic potential of APCs in cancer treatment.

Here, we aimed to understand the effect of the APC miltefosine (HePC) on membrane fluidity in A549 cancer cells compared to normal endothelial cells (human umbilical vein endothelial cells (HUVECs)). For this purpose, we measured cholesterol and sphingomyelin levels in HePC-treated cells and performed fluorescence recovery after photobleaching (FRAP) analysis using fusogenic liposomes [11] under physiological conditions. This study supports the selective action of HePC on cancer cell membranes and its potential as an antitumor lipid.

Materials and Methods

Chemicals

Miltefosine (hexadecylphosphocholine (HePC)) (cat. No.: HY-13685) was purchased from MedChemExpress (Monmouth Junction, NJ, USA). 1,2-dioleoyl-3-trimethylammonium propane (DOTAP) (cat. No. 890890), and 1,2-dioleoyl-sn-glycero-3-phosphoethanolamine (DOPE) (cat. No. 850725) were from Avanti Polar Lipids (Alabaster, AL, USA). DiD (cat. No. 42364) was from Sigma-Aldrich Co. LLC (St. Louis, MO, USA).

Cell Culture

Human lung adenocarcinoma (A549) and HUVEC cells (ATCC, Manassas, VA, USA) were cultured at 37 °C in a humidified atmosphere containing 5% CO_2 in Dulbecco's Modified Eagle Medium (DMEM) (cat. No. 30-2002, ATCC), supplemented with 10% Fetal bovine serum (FBS) (cat. No. F7524), 1 mM L-glutamine (cat. No. G7513) and Penicillin/Streptomycin/amphotericin B (100 units/mL: 10 mg/mL: 25 µg/mL) (cat. No. A5955) all acquired from Sigma-Aldrich Co. LLC. Cells were passaged every 3–5 days and were routinely checked for mycoplasma contamination via MycoStrip™ mycoplasma detection kit (cat. No. rep-mysnc-50, InvivoGen, Toulouse, France). Cells were confirmed by cytomorphologic observation and surface marker identification.

Cell Viability

The 3-(4,5-dimethylthiazol-2-yl)-2,5-diphenyl-2H-tetrazolium bromide (MTT) cell viability assay was used to determine the half-maximal inhibitory concentration (IC_{50}) of HePC [12]. Briefly, cells were seeded in 96-well plates (1×10^4 cells/well), incubated for 24 h to allow them to adhere, and then treated for 24 h with HePC at different concentrations (100–300 µM for A549 cells; 20–200 µM for HUVEC cells). Following the incubation period, cells were stained with MTT reagent (5 mg/mL in phosphate-buffered saline) for 3 h, 37 °C, and 5% CO_2, the formazan crystals that formed were then dissolved in 5% formic acid in isopropanol and measured spectrophotometrically at 570 nm using a microplate reader (Tecan Infinite F200 PRO, Tecan Group Ltd., Männedorf, Switzerland). Cell viability was normalized to the absorbance of the control samples (100% viable). The normalized cell viability was used to determine the half-maximal inhibitory concentration (IC_{50}) values by non-linear regression analysis using log(inhibitor) vs normalized response, variable slope in GraphPad Prism version 5.0 software (GraphPad Software, Inc., La Jolla, CA, USA) from three independent experiments in which each sample was repeated in triplicate.

Determination of Total Cholesterol and Sphingomyelin

Total cholesterol was measured using a Cholesterol Assay Kit (ab65390, Abcam, Cambridge, UK) according to the manufacturer's instructions with a few modifications. Cells were treated with IC_{50} concentrations of HePC (180 µM for A549, 80 µM for HUVEC) for 24 h, harvested, washed with ice-cold phosphate-buffered saline, the cell pellets (2×10^6 cells) were resuspended in chloroform: isopropanol: Triton X-100 (7:11:0.1) and homogenized with a SONOPULS ultrasonic homogenizer (BANDELIN electronic GmbH&Co. KG, Berlin, Germany). Lipids were extracted by centrifugation for 10 min at 15,000 g and the organic phase was transferred to a new tube and air dried at 50 °C under $N_2(g)$. The lipids were dissolved in the Assay Buffer provided with the assay kit. Absorbance was measured using a microplate reader (Tecan Infinite F200 PRO) at 570 nm.

Sphingomyelin levels were measured using a Sphingomyelin Assay Kit (ab1333118, Abcam, Cambridge, UK) with absorbance at 595 nm (Tecan Infinite F200 PRO). 2×10^6 cells were pelleted after 24 h treatment with HePC (180 µM for A549, 80 µM for HUVEC), resuspended in the assay buffer provided with the kit and incubated for 2 h at 4 °C under constant agitation. The supernatant was separated after centrifugation at 10,000 g, 4 °C, 20 min. Afterward, the supernatant was heated for 5 min at 70 °C twice and centrifuged at 10,000 g for 2 min to remove cell debris.

Both cholesterol and sphingomyelin levels were assayed in two independent experiments and each sample was

measured in triplicate. The lipid levels were quantified using a designated standard curve and by taking into account the background absorption and the dilution factor of each assay. Statistical analysis was performed via GraphPad Prism version 5.0 software using the Mann-Whitney test.

Fluorescence Recovery after Photobleaching (FRAP)

Membrane dynamics were studied using FRAP with fusogenic liposomes. The liposomes were prepared according to the protocol by Kleusch *et al*., 2012 [11] from DOTAP:DOPE:DiD = 1:1:0.1 (w/w) with few modifications. The reagents were dissolved in chloroform and mixed in the given ratio in glass tubes. The chloroform was removed under N_2*(g)* and the resulting lipid layer was dissolved in 20 mM 4-(2-hydroxyethyl)-1-piperazineethanesulfonic acid (HEPES), pH 7, vortexed for 2 min, and incubated at 4 °C overnight for full layer rehydration. Following the incubation the solution was sonicated with SONOPULS ultrasonic homogenizer (BANDELIN electronic GmbH&Co. KG, Berlin, Germany) for 20 min on ice and used immediately or stored for up to 1 week at 4 °C. Cells were seeded on 35 mm glass-bottom Petri dishes (MatTek, Ashland, MA, USA), treated with Dimethyl sulfoxide (DMSO) or the corresponding IC_{50} HePC for 24 h (180 µM for A549, 80 µM for HUVEC). To stain the membranes, the liposomes were diluted 50-fold in serum-free media, distributed drop-wise over the cells and incubated for 15 min, 37 °C, 5% CO_2 on an orbital shaker. Following the incubation, the cell medium was refreshed and the cells were incubated for another 3 h. Imaging was done 3 h post-incubation using an Andor Revolution spinning disk confocal system (Oxford Instruments plc, Abington, UK) with a Nikon Eclipse Ti-E inverted microscope (Nikon Instruments Inc., Tokyo, Japan) equipped with the Nikon Perfect Focus System (PFS). Image acquisition was accomplished by means of a Nikon CFI Plan Apo VC 60× (NA 1.2) water immersion objective and high-sensitivity iXon897 Electron Multiplying Charge-Coupled Device (EMCCD) camera (Nikon Instruments Inc., Tokyo, Japan). FRAP experiments were performed with the Andor FRAPPA (Oxford Instruments plc, Abington, UK) photobleaching and photoactivation module. Photobleaching of the cell membrane was accomplished by the use of a 561 nm laser (Cobolt Jive™, Hübner Photonics GmbH, Kassel, Germany) with a nominal power of 50 mW attenuated to 35% with 20 repeats and 100 ms dwell time. The shape of the bleached region of interest (ROI) was circular, with a diameter of 10 pixels (2.3 µm). Image analyses were performed using the open-source CellTool software (version 1.7.0.0, Copyright (C) 2023 Georgi Danovski, https://dnarepair.bas.bg/software/CellTool/) [13]. FRAP mathematical modeling was conducted in the Results Extractor Tab in CellTool. A double exponential FRAP equation for circular ROI was applied to calculate the diffusion coefficient and the half-time of fluorescence recovery. Fusogenic liposomes were freshly prepared and applied simultaneously to control and HePC-treated samples of each cell line. Each condition was tested in at least three independent experiments. During each experiment, data from a minimum of 10 cells per condition was collected. After analysis, data from at least 20 cells per condition were further processed. Statistical comparisons between control and treated conditions were performed using the Mann-Whitney, a non-parametric method suitable for independent samples with no pairing between control and treated groups.

Results

Cell Viability of A549 and HUVEC Cells Upon HePC Treatment

To assess the cytotoxic impact of HePC on A549 and HUVEC cells, we treated both cell lines with HePC for 24 hours. By doing so, we determined the half-maximal inhibitory concentration (IC_{50}) for each cell line (Fig. 1).

The estimated IC_{50} values were 180 ± 10 µM for A549 and 80 ± 10 µM for HUVEC. These results highlight the effectiveness of HePC in inhibiting cell growth in both cancerous and normal endothelial cells. Notably, HePC is more toxic to normal endothelial cells (HUVEC) than to cancer cells (A549).

Miltefosine Alters Cholesterol Levels in A549 Cells

Fig. 2 shows the determined cholesterol and sphingomyelin levels in A549 and HUVEC cells upon HePC treatment. A comparison between treated and non-treated cells revealed an overall increase in total cholesterol in both cell lines (Fig. 2A).

For A549 cells, cholesterol concentrations were 0.3997 ± 0.02 µg/µL for the control versus 0.5923 ± 0.01 µg/µL for HePC-treated cells. In general, HUVEC cells have lower cholesterol levels, consistent with their somatic phenotype. Nevertheless, HePC increased the total cholesterol concentration from 0.2236 ± 0.002 µg/µL to 0.2649 ± 0.002 µg/µL. Sphingomyelin levels in A549 cells remained largely unchanged, averaging 67.1 ± 2.6 mg/dL and 66.8 ± 5.4 mg/dL for untreated and HePC-treated cells, respectively (Fig. 2B). In contrast, in HUVEC cells, HePC caused a decrease in sphingomyelin from 43.45 ± 1.2 mg/dL to 30.8 ± 2.06 mg/dL.

Miltefosine Reduces Membrane Fluidity in A549 Cells

To investigate the impact of HePC on membrane dynamics, we employed a FRAP approach, which allows us to measure the lateral diffusion of lipids within the cell membrane. Cell membranes were fluorescently labeled with fusogenic liposomes [11], and a section of the membrane was irradiated with a focused laser beam until the complete loss of fluorescence (Fig. 3A,D). The recovery time of the signal at the same location was then determined (Fig. 3B,E).

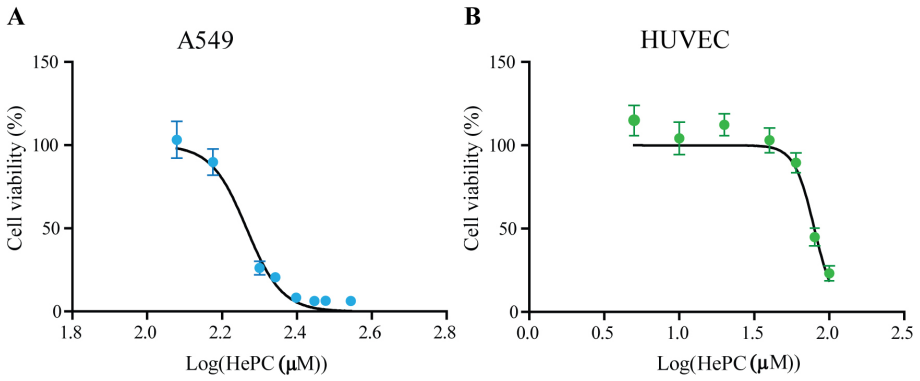

Fig. 1. Cell viability of (A) A549 cells and (B) HUVECs treated with HePC for 24 hours. Half-maximal inhibitory concentration (IC_{50}) values were estimated with a nonlinear regression curve fit: log(inhibitor) vs normalized response – variable slope. The concentration range of HePC is presented as log (HePC (μM)). Calculated Log(IC_{50}) values of three independent replicates: Log(IC_{50}) for A549 = 2.255 (95% confidential interval is between 2.230–2.740); Log(IC_{50}) for HUVEC = 1.903 (95% confidential interval is between 1.849–1.955). The experiment was performed in triplicates. A549 cells, human lung adenocarcinoma cells; HUVECs, human umbilical vein endothelial cells; HePC, hexadecylphosphocholine.

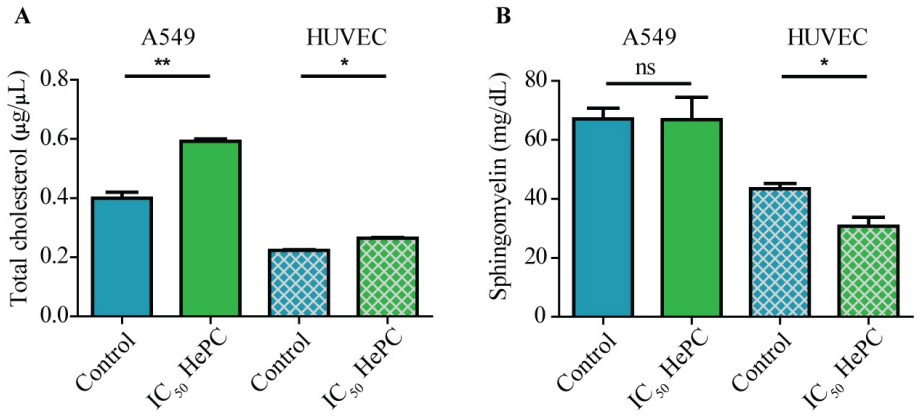

Fig. 2. Miltefosine alters cholesterol levels in A549 cells. A549 and HUVEC cells treated with IC_{50} HePC for 24 hours – (A) total cholesterol and (B) sphingomyelin concentrations. Bar charts depict Mean ± SEM. Statistical analysis - Mann-Whitney test; *$p < 0.05$, **$p < 0.01$, ns, not significant. The experiment was performed in two independent experiments and each sample was measured in triplicate.

The movies of the recovery kinetics of the cells after irradiation can be found in **Supplementary Materials** (movies related to Fig. 3). By analyzing the recovery kinetics, we calculated the diffusion coefficient (D) and half-time of fluorescence recovery ($\tau_{1/2}$), which serve as indicators of the degree of membrane organization and fluidity (Fig. 3C,F). FRAP experiments were performed on adherent cells by fluorescence spinning disk confocal microscopy under *in vivo* conditions (37 °C, 5% CO_2), providing an optimal physiological environment for cell viability and ensuring accurate measurements.

Under the action of HePC, the membranes of cancer cells underwent a change in their fluidity, in contrast to non-cancerous cells (Fig. 3C,F). Data from FRAP analysis showed a significant decrease in the diffusion coefficient in A549 cells after IC_{50} HePC treatment ($p < 0.001$), while a smaller, but still statistically significant, reduction was observed in HUVEC cells ($p < 0.05$). Analogously, the half-time of fluorescence recovery increased for A549 and showed a slight, non-significant increase in HUVECs.

Discussion

The obtained higher toxicity of HePC to HUVECs raises concerns regarding its safety use and explains some of the documented side effects of the drug. Previous studies have also reported the high cytotoxicity of HePC against non-cancerous cells such as erythrocytes (high hemolytic potential) and macrophages [4]. In addition, supporting our findings, Zerp *et al.*, 2008 [14] demonstrated that HePC induces apoptosis and inhibits tube formation in endothelial cells, suggesting that HePC is capable of interfering with angiogenesis *in vitro* which on the other hand could benefit the antitumor effect of HePC.

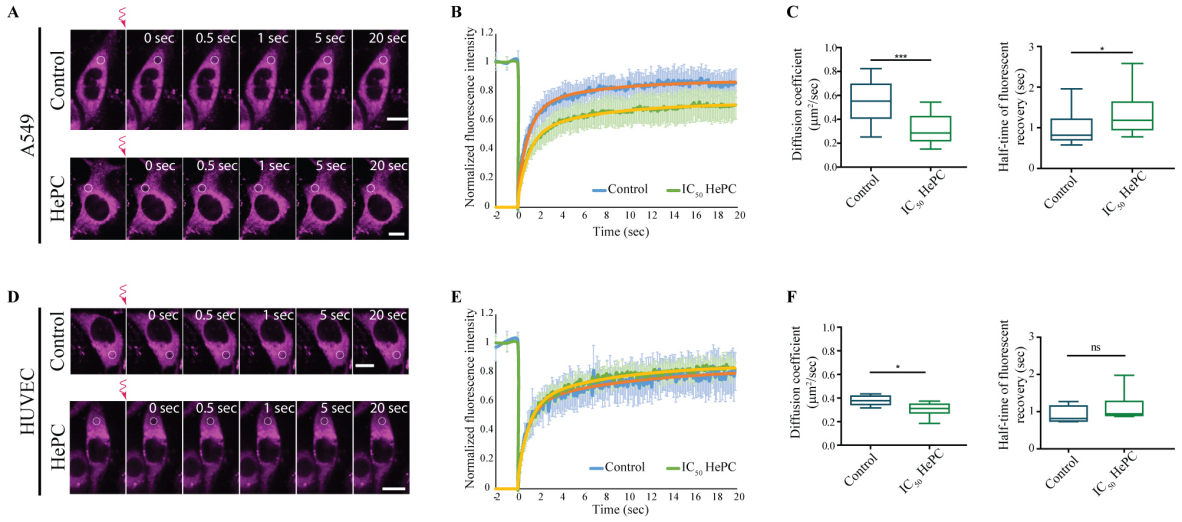

Fig. 3. Miltefosine reduces membrane fluidity in A549 cells but has little effect in HUVEC. (A–C) A549 cell line. (D–F) HUVEC cell line. (A,D) Fluorescence recovery after photobleaching (FRAP) imaging of control and treated cells. Scale bar = 10 μm. The bleached region of interest is marked with dashed circles. (B,E) Normalized fluorescence intensity after photobleaching. Fitted curves are shown with orange (control) and yellow (HePC) lines. (C,F) Diffusion coefficient (μm^2/sec) and FRAP half-times (sec), estimated via FRAP modeling. Statistical analysis - Mann-Whitney test; ns, non significant; *$p < 0.05$, ***$p < 0.001$. n = 20 cells per condition.

Cholesterol and sphingomyelin play an essential role in cell signaling by forming membrane microdomains known as lipid rafts. Alterations in their normal concentrations in cell membranes could disrupt the rafts, change membrane fluidity, and impact processes such as cell proliferation, migration, and apoptosis. Park *et al.* [15] reported that HePC modulates cell proliferation and survival by interacting with lipid rafts in a cholesterol-dependent manner. The cholesterol level in the cell membrane is critical for various cell functions. For instance, low cholesterol levels typically result in increased membrane fluidity and may promote metastasis. Conversely, elevated cholesterol levels are associated with a higher order of lipid packing, increased membrane rigidity, reduced permeability, and enhanced drug resistance [5]. Also, cholesterol has been shown to protect model membranes against membrane lipid degradation [16]. The obtained much higher increase in the cholesterol level of A549 cells after HePC treatment than that for HUVECs may lead us to assume that treatment of cancer cells with HePC may cause membrane stiffness. This assumption is also supported by the FRAP analysis. These results suggest that HePC makes the membrane of A549 cells substantially more rigid while having a lesser effect on the non-cancerous HUVEC cells. Given that cancer cells, in general, have softer membranes, allowing them to migrate faster and metastasize [5,17], we could speculate that HePC could reduce the metastatic potential of A549 cells.

The reductions in sphingomyelin are often associated with an increase in ceramide. The latter is a structural and signaling lipid molecule that can promote cell death through apoptosis [18]. Thus, the reduction of sphingomyelin level in HUVEC cells after HePC treatment may contribute to the sensitivity of these cells to the drug, as confirmed by the higher cytotoxicity to endothelial cells shown by the MTT assay.

In addition to their use for membrane staining and analysis, fusogenic liposomes have been identified as promising drug carriers with tunable membrane fluidity [19]. Bompard *et al.*, 2020 [19] demonstrated that liposomes with lower membrane rigidity preferentially fuse with cancer cells and exhibit greater cytotoxicity toward them compared to normal cells. This suggests that membrane fluidity, rather than specific protein interactions, can play a critical role in influencing drug targeting, administration, and antitumor activity. Building on this concept, our approach to studying membrane-targeting drugs could provide valuable insights into how they affect membrane fluidity, while also aiding in the development of novel, selective drug delivery systems. In this regard, the concept of developing formulations of miltefosine-loaded polymeric micelles or particles [20] will be useful to mitigate the drug's toxic effects on healthy cells and increase its selectivity to cancer cells.

Conclusion

Miltefosine reduces membrane fluidity in the A549 cancer cell line, leading to increasing membrane rigidity. Changes in the diffusion coefficient were also observed in the non-cancerous HUVEC cells, but the alterations were more pronounced in A549 cells. These findings suggest that miltefosine's mechanism of action involves altering the biophysical properties of lipid membranes, with a stronger

impact on cancer compared to non-cancerous cells. The decreased levels of sphingomyelin and high cytotoxicity to endothelial cells may be a sign of miltefosine's interference with angiogenesis, which may contribute to the additional antitumor effect of this agent. Considering the different membrane fluidity of cancer and endothelial cells and the need to avoid the hemolytic effect of miltefosine, different strategies for its incorporation into drug carriers can be explored.

Availability of Data and Materials

The datasets used and/or analyzed during the current study are available from the corresponding author upon reasonable request.

Author Contributions

RT and IG designed the research study. IG, SA and TV performed the research. KK validated the research and provided help and advice on the writing and editing of the manuscript. IG analyzed the data. IG and RT wrote the manuscript. All authors were involved in the drafting and critical revision of the manuscript. All authors have read and approved the final manuscript. All authors have participated sufficiently in the work and agreed to be accountable for all aspects of the work.

Ethics Approval and Consent to Participate

Not applicable.

Acknowledgment

The authors are grateful to Prof. Albena Momchilova, DSc from the Institute of Biophysics and Biomedical Engineering at the Bulgarian Academy of Sciences for the materials provided for the study.

Funding

All authors are grateful to HE project ENSIGN #101086226 (HORIZON-MSCA-2021-SE-01) Emerging nanoscopy for single entity characterization as well as the Bulgarian Advanced Light Microscopy node of the Euro-Bioimaging Consortium, proposal ID 2180. Georgieva I. acknowledges the support of the National Research Programme "Young scientists and post-doctoral students", DCM #577, Bulgarian Ministry of Education.

Conflict of Interest

The authors declare no conflict of interest.

Supplementary Material

Supplementary material associated with this article can be found, in the online version, at https://doi.org/10.24976/Discov.Med.202537194.45.

References

[1] Marguet D, Lenne PF, Rigneault H, He HT. Dynamics in the plasma membrane: how to combine fluidity and order. The EMBO Journal. 2006; 25: 3446–3457.

[2] Alves AC, Ribeiro D, Horta M, Lima JLFC, Nunes C, Reis S. A biophysical approach to daunorubicin interaction with model membranes: relevance for the drug's biological activity. Journal of the Royal Society, Interface. 2017; 14: 20170408.

[3] Pehlivanova V, Uzunova V, Tsoneva I, Berger, MR, Ugrinova I, Tzoneva R. Effect of Erufosine on the Reorganization of Cytoskeleton and Cell Death in Adherent Tumor and Non-Tumorigenic Cells. Biotechnology & Biotechnological Equipment. 2013; 27: 3695–3699.

[4] Kostadinova A, Topouzova-Hristova T, Momchilova A, Tzoneva R, Berger MR. Antitumor Lipids–Structure, Functions, and Medical Applications. Advances in Protein Chemistry and Structural Biology. 2015; 101: 27–66.

[5] Szlasa W, Zendran I, Zalesińska A, Tarek M, Kulbacka J. Lipid composition of the cancer cell membrane. Journal of Bioenergetics and Biomembranes. 2020; 52: 321–342.

[6] Çetinel ZÖ, Bilge D. The effects of miltefosine on the structure and dynamics of DPPC and DPPS liposomes mimicking normal and cancer cell membranes: FTIR and DSC studies. Journal of Molecular Liquids. 2022; 356: 119041.

[7] Çetinel ZÖ, Bilge D. Investigation of miltefosine-model membranes interactions at the molecular level for two different PS levels modeling cancer cells. Journal of Bioenergetics and Biomembranes. 2024; 56: 461–473.

[8] Alonso L, Mendanha SA, Marquezin CA, Berardi M, Ito AS, Acuña AU, *et al*. Interaction of miltefosine with intercellular membranes of stratum corneum and biomimetic lipid vesicles. International Journal of Pharmaceutics. 2012; 434: 391–398.

[9] Uzunova V, Tzoneva R, Stoyanova T, Pankov R, Skrobanska R, Georgiev G, *et al*. Dimethylsphingosine and miltefosine induce apoptosis in lung adenocarcinoma A549 cells in a synergistic manner. Chemico-biological Interactions. 2019; 310: 108731.

[10] Tzoneva R, Stoyanova T, Petrich A, Popova D, Uzunova V, Momchilova A, *et al*. Effect of Erufosine on Membrane Lipid Order in Breast Cancer Cell Models. Biomolecules. 2020; 10: 802.

[11] Kleusch C, Hersch N, Hoffmann B, Merkel R, Csiszár A. Fluorescent lipids: functional parts of fusogenic liposomes and tools for cell membrane labeling and visualization. Molecules (Basel, Switzerland). 2012; 17: 1055–1073.

[12] Mosmann T. Rapid colorimetric assay for cellular growth and survival: application to proliferation and cytotoxicity assays. Journal of Immunological Methods. 1983; 65: 55–63.

[13] Danovski G, Dyankova-Danovska T, Stamatov R, Aleksandrov R, Kanev PB, Stoynov S. CellTool: An Open-Source Software Combining Bio-Image Analysis and Mathematical Modeling for the Study of DNA Repair Dynamics. International Journal of Molecular Sciences. 2023; 24: 16784.

[14] Zerp SF, Vink SR, Ruiter GA, Koolwijk P, Peters E, van der Luit AH, *et al*. Alkylphospholipids inhibit capillary-like endothelial tube formation in vitro: antiangiogenic properties of a new class of antitumor agents. Anti-cancer Drugs. 2008; 19: 65–75.

[15] Park SY, Kim JH, Choi JH, Lee CJ, Lee WJ, Park S, *et al*. Lipid raft-disrupting miltefosine preferentially induces the death

of colorectal cancer stem-like cells. Clinical and Translational Medicine. 2021; 11: e552.

[16] Zhang X, Barraza KM, Beauchamp JL. Cholesterol provides nonsacrificial protection of membrane lipids from chemical damage at the air-water interface. Proceedings of the National Academy of Sciences of the United States of America. 2018; 115: 3255–3260.

[17] Preta G. New Insights Into Targeting Membrane Lipids for Cancer Therapy. Frontiers in Cell and Developmental Biology. 2020; 8: 571237.

[18] Alizadeh J, da Silva Rosa SC, Weng X, Jacobs J, Lorzadeh S, Ravandi A, *et al*. Ceramides and ceramide synthases in cancer: Focus on apoptosis and autophagy. European Journal of Cell Biology. 2023; 102: 151337.

[19] Bompard J, Rosso A, Brizuela L, Mebarek S, Blum LJ, Trunfio-Sfarghiu AM, *et al*. Membrane Fluidity as a New Means to Selectively Target Cancer Cells with Fusogenic Lipid Carriers. Langmuir: the ACS Journal of Surfaces and Colloids. 2020; 36: 5134–5144.

[20] Valenzuela-Oses JK, García MC, Feitosa VA, Pachioni-Vasconcelos JA, Gomes-Filho SM, Lourenço FR, *et al*. Development and characterization of miltefosine-loaded polymeric micelles for cancer treatment. Materials Science & Engineering. C, Materials for Biological Applications. 2017; 81: 327–333.